

Actin-based propulsion of spatially extended objects

Mihaela Enculescu^{1,3} and Martin Falcke²

¹ Institute for Theoretical Physics, Technische Universität Berlin,
Hardenbergstrasse 36, 10623 Berlin, Germany

² Max-Delbrück-Center for Molecular Medicine, Mathematical Cell
Physiology, Robert-Rössle-Street 10, 13125 Berlin, Germany
E-mail: mihaela.enculescu@tu-berlin.de

New Journal of Physics **13** (2011) 053040 (13pp)


Received 16 December 2010

Published 20 May 2011

Online at <http://www.njp.org/>

doi:10.1088/1367-2630/13/5/053040

Abstract. We propose a mathematical model of the actin-based propulsion of spatially extended obstacles. It starts from the properties of individual actin filaments and includes transient attachment to the obstacle, polymerization as well as cross-linking. Two particular geometries are discussed, which apply to the motion of protein-coated beads in a cell-like medium and the leading edge of a cell protrusion, respectively. The model gives rise to both steady and saltatory movement of beads and can explain the experimentally observed transitions of the dynamic regime with changing bead radius and protein surface density. Several spatiotemporal patterns are obtained with a soft obstacle under tension, including the experimentally observed spontaneous emergence of lateral traveling waves in crawling cells. Thus, we suggest a unifying mechanism for systems that are currently described by differential concepts.

 Online supplementary data available from stacks.iop.org/NJP/13/053040/mmedia

Contents

1. Introduction	2
2. Propulsion of a rigid sphere	2
3. Propulsion of a soft membrane under tension	8
4. Conclusions	9
References	11

³ Author to whom any correspondence should be addressed.

1. Introduction

Cell migration is required for wound healing, immune response or metastasis. A variety of eukaryotic cells crawl by extending a thin plane cytoskeleton structure, the lamellipodium, in the direction of motion. The growth of a cross-linked actin network through polymerization behind its leading edge membrane generates the protrusion force that pushes the lamellipodium forward.

The actin cytoskeleton also determines the dynamics of the lamellipodium shape. Quantitative analysis has revealed that in a variety of crawling cells protrusion and retraction events at the leading edge are organized in lateral waves along the cell membrane and that the wave pattern can be changed by activating signaling molecules [1, 2]. Therefore, actin dynamics generates spatial and temporal structures and cell morphology could be used to reveal the state of the cytoskeleton without direct intervention if the emergence of different morphodynamic patterns were well understood. However, current models show either steady motion only or require myosin activity for these spatiotemporal dynamics, which is in contrast to experimental observations. We present a model reproducing the observed wave patterns in compliance with the experimental conditions. The local dynamics of the model is described below and was developed in [3]. Here, we apply it to spatially extended systems.

Protein-coated beads are used to reconstitute actin-based motility [4, 5], since they can hijack, like bacteria, the actin-based machinery of the cell for propulsion leaving behind a tail of actin polymers. The regime of motion (steady or oscillatory) depends on the bead diameter as well as on the surface density of the protein activating actin polymerization. Bead motion has been described by gel continuum theory [4]. Velocity oscillations were explained by a periodic relaxation of the stress in the gel-like actin tail resulting from polymerization [4]. The motility of beads has been also reconstituted *in silico* [6]. This approach uses a network realization of the elastic gel model and can explain the symmetry breaking of the actin cloud at the initiation of motion as well as the different regimes of motion. It predicts a transition from smooth to pulsatile motion with increasing degree of network cross-linking or increasing friction [6]. However, size dependence of the dynamic state is not discussed.

Hence, despite the similarity between the molecular constituents of lamellipodium and bead motion, they are currently described by different modeling concepts (elastic gel versus filament models) and their velocity oscillations are explained by different mechanisms. The following approach captures both the shape dynamics of lamellipodia and bead propulsion. It thus suggests a unifying mechanism for both systems, expands lamellipodium theory by shape dynamics and provides a microscopic description of the bead motion.

2. Propulsion of a rigid sphere

When beads coated with proteins that activate actin polymerization are placed in a cell-like medium, they start to assemble an actin gel, resulting in a symmetric actin cloud surrounding the bead. After 3–25 min, the symmetry of this cloud is broken [7], and an actin comet tail propelling the bead develops [4]. This comet tail consists of cross-linked actin filaments [8]. Some degree of cross-linking is always given due to branching. The motility assay used for the bead experiments also contained cross-linker molecules (α -actinin) [4, 9]. In analogous experiments with bacteria, it was found that their motion may (*Escherichia coli IcsA*) or may not (*Listeria*) require cross-linkers [10]. However, bacteria without cross-linkers drifted in the

medium [10], since the comet tail was not anchored. Hence, the function that we attribute to cross-linking, which is to provide support and anchoring to the filaments, appears precisely to be its function in bacteria propulsion. Interestingly, it has been shown that polymerization and cross-linking (by fascin in this case) are sufficient for *Listeria* propulsion [11], which is in agreement with our model.

The comet tail interacts with the bead surface through the brush formed by the not yet cross-linked ends of the polymers. We use, in our model of bead motion, a polymer brush with filaments aligned parallel to the direction of motion (figure 1). This is of course a simplification when compared with to the range of angles seen in experiments. It is justified by the finding that an oscillatory regime exists for a large range of orientation angles [12], and the parallel filaments appear to have a prominent role in propulsion [11, 13]. Additionally, a broad range of angles between the obstacle surface and the filaments—which is the relevant angle—are anyway included in our calculations owing to the spherical shape of the beads.

Based on the processes explained in figure 1, the dynamics of the bead+actin system can be described by the set of equations [3]

$$\begin{aligned}
 \partial_t n_a &= -k_d(l_a, \zeta) n_a + k_a n_d, \\
 \partial_t l_d &= v_p(l_d, \zeta) - \tilde{v}_g(l_d) + k_d n_a (n_d)^{-1} (l_a - l_d), \\
 \partial_t l_a &= -\tilde{v}_g(l_a) + k_a n_d (n_a)^{-1} (l_d - l_a), \\
 \partial_t y_g &= n^{-1} [v_g(l_a) n_a + v_g(l_d) n_d], \\
 \partial_t y_0 &= \frac{1}{2\pi \eta R} \int_0^{2\pi} R^2 d\varphi \int_0^{\pi/2} d\theta \sin \theta \cos^2 \theta f(l_a, l_d, \zeta, \theta), \\
 f &= [n_a f_a(l_a, \zeta, \theta) + n_d f_d(l_d, \zeta, \theta)], \\
 \zeta &= (y_0 - R \cos \theta - y_g) \cos \theta \\
 \tilde{v}_g(l) &= \max(1, (l \cos \theta) \zeta^{-1}) v_g(l).
 \end{aligned} \tag{1}$$

We assume rotational symmetry with respect to the y -axis. Here, $n_a(\theta, \varphi, t)$ and $n_d(\theta, \varphi, t)$ are the surface densities of attached and detached filaments, respectively. The total surface density of filaments $n = n_a + n_d$ is assumed to be constant. $l_d(\theta, \varphi, t)$ and $l_a(\theta, \varphi, t)$ denote the average free lengths of detached and attached filaments, measured from the gel front to the tip. y_0 describes the position of the bead and $y_g(\theta, \varphi, t)$ the boundary of the cross-linked gel.

It has been shown experimentally that some filaments are attached to the bead [14]. Filaments attach to the bead surface with a constant rate k_a [15]. The detachment rate k_d increases exponentially with the pulling force exerted by attached filaments on the bead [15, 16].

The boundary of the gel advances by cross-linking of filaments at velocity v_g , which depends on the free length of the filament like $v_g^{\max} \tanh(l/\bar{l})$ [17]. The velocity \tilde{v}_g describes the shortening of the free filament length due to cross-linking. When filaments are longer than the distance to the bead surface, they buckle, and the shortening velocity is greater than the cross-linking velocity. Detached filaments polymerize with the polymerization speed v_p , which decreases exponentially with the force between the filament and the bead: $v_p = v_p^{\max} \exp(-f_d \delta \cos \theta / k_B T)$. Here, δ denotes the size of an actin monomer. Thus, the free length of the filaments can change due to processes at both ends: polymerization of the tip increases the free length, whereas cross-linking at the advancing gel boundary decreases it.

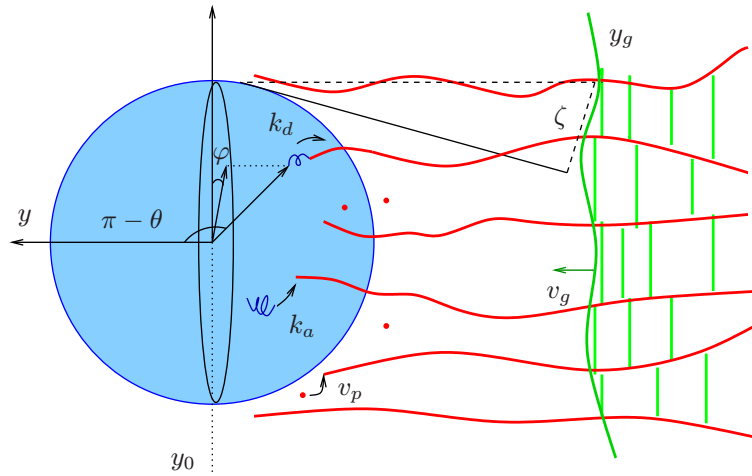


Figure 1. Side view of a bead propelled by an actin comet: actin filaments cross-link and build a gel. y_g denotes the boundary of the cross-linked gel. Polymer tips stick out of this gel. The thermal fluctuation of the polymer tips is restricted by the presence of the bead, resulting in an entropic force between the bead and the actin network that leads to bead movement. The force depends on the distance ζ between the fixed end of the filament and the local tangent to the bead at its free end. The cross-linked actin gel provides support for the filaments. Actin polymerizes at the bead surface at velocity v_p and cross-links at velocity v_g , so that the actin comet follows the bead in its movement. Filaments attach to the bead surface with rate k_a , and attached filaments detach with rate k_d .

The variable ζ denotes the minimal distance between the fixed end of a filament and the local tangent to the bead at its free end (see figure 1), and is needed for the calculation of the force exerted by filaments on the bead. For detached filaments, the free fluctuating filament end can hit the membrane and transfer mechanical momentum. The average normal force experienced by the membrane can be derived from the probability density distribution $P(l_d, \zeta, \theta)$ of the end-to-end distance:

$$f_d(l_d, \zeta, \theta) = k_B T \frac{\partial \ln P(l_d, \zeta, \theta)}{\partial \zeta}.$$

The scale of the resulting force is given by the Euler buckling force $f_c = k_B T l_p / l^2$ (l_p is the persistence length). We use the results derived in [12] in the weakly bending rod approximation. The derivation shows that for small compression $\xi = l_p(l_d - z) / l_d^2 \leq 0.2$ the scaled force reads

$$\tilde{F}_d = \frac{4 \exp(-\frac{1}{4\xi})}{\pi^{5/2} \xi^{3/2} \left[1 - 2 \operatorname{erfc} \left(\frac{1}{2\sqrt{\xi}} \right) \right]}$$

and for strong compression

$$\tilde{F}_d = \frac{1 - 3 \exp(-2\pi^2 \xi)}{1 - \frac{1}{3} \exp(-2\pi^2 \xi)}.$$

Table 1. Parameter values. References are given for those deduced from the literature. The other parameters are chosen to fit experimentally observed motion.

Parameter	Figure 2	Figure 4
Actin monomer radius, δ	2.7 nm [29]	2.7 nm [29]
Persistence length, l_p	15 μm [30]	15 μm [30]
Attachment rate, k_a	$3 \times 10^{-4} \text{ s}^{-1}$	2.16 s^{-1}
Detachment constant, k_d^0	$7 \times 10^{-3} \text{ s}^{-1}$	2 s^{-1}
Satur. cross-link. vel., v_g^{max}	$0.6 \mu\text{m min}^{-1}$	$4.5 \mu\text{m min}^{-1}$
Satur. cross-link. length, \bar{l}	100 nm	100 nm
Satur. polym. vel., v_p^{max}	$1\text{--}2.5 \mu\text{m min}^{-1}$ [31]	$6.6\text{--}9 \mu\text{m min}^{-1}$ [32, 33]
Total filament density, n	$100\text{--}500 \mu\text{m}^{-2}$	$100 \mu\text{m}^{-2}$ [34]
Orientation angle, θ_0	0°	35° [23, 24]
Linker spring constant, k_l	1 pN nm^{-2} [15, 16]	0.7 pN nm^{-2} [15, 16]
Effective drag coefficient, η	$2.25 \text{ nN}\cdot\text{s } \mu\text{m}^{-2}$ [28]	$2 \text{ pN}\cdot\text{s } \mu\text{m}^{-2}$

Further, we assume that detached filaments can transiently attach to the membrane via linker proteins that behave like elastic springs. We identify three regimes for the force f_a exerted by the serial arrangement of filaments and the linker. Depending on the relation among the distance to the membrane ζ , the projection $R_{||}$ of the equilibrium end-to-end distance onto the membrane normal and the contour length, we have: compressed filaments pushing the membrane; filaments and the linker pulling the membrane while being stretched together; or fully stretched filaments with the linker pulling the membrane while being stretched further:

$$f_a(l_a, \zeta, \theta) = \begin{cases} -k_{||}(\zeta - R_{||}), & \zeta \leq R_{||}, \\ -k_{\text{eff}}(\zeta - R_{||}), & R_{||} < \zeta < l_a \cos \theta, \\ -k_l(\zeta - l_a \cos \theta) - k_{\text{eff}}(l_a \cos \theta - R_{||}), & \zeta \geq l_a \cos \theta. \end{cases}$$

Here $k_{||}$, k_l and $k_{\text{eff}} = k_{||}k_l/(k_{||} + k_l)$ are the linear elastic coefficients of the polymer, the linker and the serial filament–linker arrangement, respectively. $k_{||}$ itself is a function of polymer stiffness and incidence angle [18]. For the range of polymer lengths obtained in the simulations discussed below, $k_{||}$ is about one order of magnitude smaller than the value estimated for k_l (see table 1). Therefore, $k_{\text{eff}} \approx k_{||}$ most of the time. The forces exerted by both the detached and the attached filaments are highly sensitive to the free length of the filament: f_d scales like $1/l^2$ and $k_{||}$ scales like $1/l^4$.

Finally, the active forces exerted by attached and detached filaments are balanced by the friction force experienced by the bead. It is mainly the force required to push the bead through the gel formed on the side of the bead facing in the direction of motion and around the equator. That friction mainly occurs in a strip along the equator of the bead [4]. The total friction force is therefore proportional to the bead radius. This linear dependence of the total friction force on the radius implies that our results also apply if the resistance to motion arises from Stoke's law. This is suggested by studies considering cross-linked actin networks as viscous fluids on the time scales relevant here [19, 20].

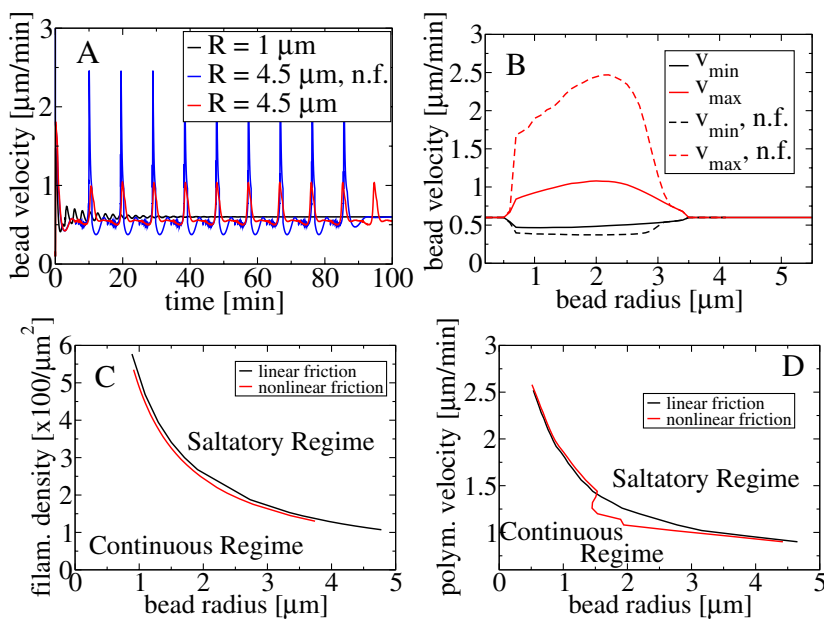


Figure 2. (A) Bead velocity for two different values of the bead radius and with nonlinear friction ($n = 500 \mu\text{m}^2$, $v_p^{\text{max}} = 1.8 \mu\text{m min}^{-1}$, see table 1 for parameter values). (B) Maximal and minimal velocities of the beads depending on the bead radius for $n = 1000 \mu\text{m}^2$, $v_p^{\text{max}} = 1.8 \mu\text{m min}^{-1}$ and linear/nonlinear friction. (C, D) Bifurcation diagrams of bead motion. (C) Variable radius and filament density and constant polymerization velocity $v_p^{\text{max}} = 1.8 \mu\text{m min}^{-1}$. (D) Variable radius and polymerization velocity and constant filament density $n = 500 \mu\text{m}^2$.

Figure 2(A) shows the solutions of equations (1). Small beads move steadily, but the velocity of larger ones oscillates. The oscillation mechanism is based on periodic and sudden detachment of attached filaments from the bead surface. In the first phase of an oscillation cycle, there is a large number of attached filaments, which pull back the bead. When the bead velocity becomes lower than the growth velocity of the gel, the filaments get compressed, and the polymerization velocity decreases due to its force dependence. When the polymerization velocity of the tip becomes less than the velocity of the gel front, the free part of the filament shrinks. As a result, the forces between the filaments and the bead increase further, which leads to further shortening of the filaments. This ends in the explosive detachment of filaments, due to the force dependence of the detachment rate k_d . Detached filaments are still very short, exerting a strong pushing force, which accelerates the bead movement. If the total pushing force exerted at this time is strong enough, the bead escapes the gel and becomes, for a short time, faster than the gel growth velocity. In a second phase, the filaments relax, grow at their maximum polymerization speed, and initially do not stay attached to the bead, since the detachment rate is still very high. As the filaments grow longer, the magnitude of the forces decreases, leading to a reduced detachment rate. The filaments attach to the bead and slow it down, and the cycle is repeated.

Figure 2(B) shows the dependence of bead velocity on radius. After the onset of oscillatory movement, the amplitude of the oscillations increases up to a maximum and then decreases again, and finally, a second transition back to steady movement is obtained.

Figures 2(C) and (D) show state diagrams of the system, very similar to the state diagram measured in [4]. The authors of [4] state that the surface concentration of the protein activating actin polymerization is also able to induce transitions between steady and oscillatory bead movements. Protein surface concentration is revealed by the total filament density in our model. Increasing it induces a Hopf bifurcation, resulting in a transition from steady to saltatory motion (see figure 2(C)). The transition can also be achieved by increasing the polymerization rate (see figure 2(D)).

The oscillatory movement arises when two critical conditions are met: (i) short detached filaments must be strong enough to accelerate the bead above the gel growth velocity, once explosive detachment occurs at the end of the compression phase. (ii) The attachment of filaments must be strong enough to decelerate the bead below the gel growth velocity at the end of the relaxation phase. Therefore, the total force per filament has to exceed the critical value $6\pi\eta Rv_g/\pi R^2n \sim 1/nR$ to initiate the relaxation phase and has to decrease below this value again to initiate the compression phase. The force exerted by a single filament depends critically on its length and is influenced mainly by the internal model parameters such as the polymerization speed and the detachment rate. The geometric parameter R has only a weak influence on this force. It follows intuitively that if all other parameters are fixed, the two transitions between oscillatory and steady regimes occur along $n \sim 1/R$. The state diagram in [4] shows only the first changes in the dynamic regime from steady to oscillatory with increasing bead radius. However, the experimentally available range for the protein surface concentration is limited by a saturation value. The second transition line predicted by our model lies, for the examined bead sizes, above the domain shown in figure 2(C). We believe therefore that this second transition corresponds to experimentally inaccessible concentrations above the saturation value in [4]. Still, a second transition might be observable for other motility assays.

The average velocity and the period (~ 10 min) agree excellently with experiments, while the oscillation amplitude ($\sim 0.5 \mu\text{m min}^{-1}$) is about one-half the reported experimental value [4]. The correct amplitude can be attained if nonlinear friction (n.f.) F_f is included. Bernheim-Groswasser *et al* [4] showed that this nonlinear friction may apply to bead motion. This type of friction is characteristic of the relative movement of sticky objects such as e.g. a violin string and the bow [21]. Nonlinear friction can be induced also when treating the gel as a viscous fluid. In this case, the coefficient η is an effective friction coefficient given by the viscosity of the gel, the viscosity of the surrounding fluid and the geometry of the actin cloud. During the oscillation cycle, the bead experiences a drop in the effective friction coefficient after it partially escapes the highly viscous actin cloud following the breaking of filament attachments. The nonlinear friction increases the amplitude of the velocity spikes, but does not change their frequency or width.

In the examples of figure 2, the friction force was assumed to be piecewise linear, with the friction coefficient η changing to $\eta/2$ when \dot{y}_0 increases above a threshold v_1 , and changing back to η when \dot{y}_0 decreases below a second threshold v_2 . v_1 and v_2 were chosen to fit the experimentally measured oscillation amplitude⁴.

The velocity in the steady regime is independent of the bead radius, in agreement with measurements [22].

⁴ $F_f = \eta\dot{y}_0$, $\dot{y}_0 \leq v_1$; $0.5\eta\dot{y}_0$, $\dot{y}_0 \geq v_2$; $\eta((0.5v_2 - v_1)\dot{y}_0 + 0.5v_2v_1)/(v_2 - v_1)$, otherwise; $v_1 = 0.78 \mu\text{m min}^{-1}$, $v_2 = 0.96 \mu\text{m min}^{-1}$.

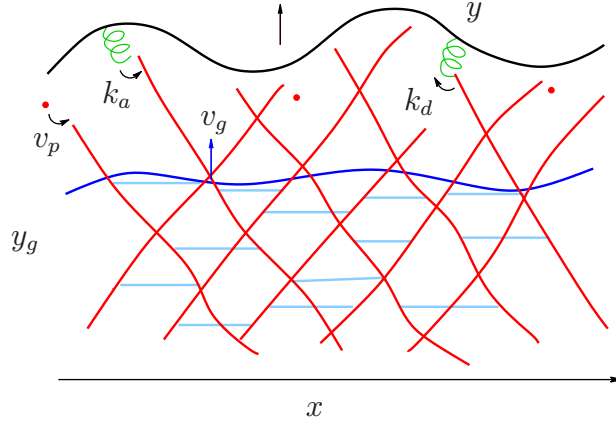


Figure 3. Top view of the lamellipodium: the actin network behind the membrane $y(x)$ has two structurally different parts: the cross-linked gel, toward the cell center, and the brush of free polymer ends sticking out of the gel, toward the cell membrane. The boundary between the brush and the gel is described by $y_g(x)$. Filaments attach to the membrane at the rate k_a , and attached filaments detach again at the rate k_d . Detached filaments elongate by polymerization with velocity v_p . Cross-linker continuously binds to the free polymer ends, so that the gel boundary advances at velocity v_g .

3. Propulsion of a soft membrane under tension

In contrast to the rigid bead surface, the leading edge membrane of a lamellipodium is a soft obstacle. The model can be adapted to the lamellipodium by the inclusion of two populations of filaments $n_a^\pm(x, t)$ and $n_d^\pm(x, t)$ oriented with an angle $+\theta_0$ or $-\theta_0$ with respect to the direction of protrusion (see [23, 24]), and a flexible membrane with tension at the leading edge. These lead to the following equations, which we have previously introduced in [25]:

$$\begin{aligned}
 \partial_t n_a^\pm &= -k_d(l_a, z^\pm)n_a^\pm + k_a n_d^\pm, \\
 \partial_t l_d^\pm &= v_p(l_d^\pm, y, y_g, y_x) - \tilde{v}_g(l_d^\pm, y, y_g) + k_d n_a^\pm (n_d^\pm)^{-1} (l_a^\pm - l_d^\pm), \\
 \partial_t l_a^\pm &= -\tilde{v}_g(l_a^\pm, y, y_g) + k_a n_d^\pm (n_a^\pm)^{-1} (l_d^\pm - l_a^\pm), \\
 \partial_t y_g &= [v_g(l_a^+)n_a^+ + v_g(l_d^+)n_d^+ + v_g(l_a^-)n_a^- + v_g(l_d^-)n_d^-]/n, \\
 \partial_t y &= \frac{1}{\eta} \left[\sum_{i=a,d} \sum_{j=\pm} n_i^j f_i(l_i^j, z^j, \theta^j) + S \frac{y_{xx}}{1+y_x^2} \right], \\
 \theta^\pm &= \pm\theta_0 + \arctan y_x, \quad z^\pm = (y - y_g) \cos \theta^\pm (\cos \theta_0)^{-1}, \\
 \tilde{v}_g(l) &= \max((\cos \theta_0)^{-1}, l(y - y_g)^{-1})v_g(l).
 \end{aligned} \tag{2}$$

The direction of protrusion is defined by the direction y of the cross-linking velocity (see figure 3). The sum $n = n_a^+ + n_a^- + n_d^+ + n_d^-$ is assumed to be constant. $l_d^\pm(x, t)$ and $l_a^\pm(x, t)$ are the average free lengths of right/left-oriented detached and attached filaments. $y(x, t)$ describes the position of the membrane and $y_g(x, t)$ the boundary of the cross-linked gel (see figure 3).

Attachment, detachment, polymerization and cross-linking are as before. θ^\pm denote now the angles between the filament and the local membrane normal for right/left oriented filaments and z^\pm denote the distances from the fixed ends to the local tangent. A constant membrane tension S leads to a force resisting the bending of the membrane that is proportional to the local curvature.

In [25], we have considered the case of a symmetric network and shown that the model can reproduce the change in the morphodynamic state found experimentally between epithelial cells in control conditions and cells expressing constitutively active Rac, a signaling molecule involved in the regulation of lamellipodium network assembly. Here we outline the complete spectrum of regimes of motion and transitions shown by the model, including the interesting case of asymmetric networks.

The lamellipodium model contains two additional parameters compared to the case of a rigid obstacle: the membrane tension S and the ratio between the total densities of filaments oriented to the right and left sides. The coefficient $a = |n_a^+ + n_d^+ - n_a^- - n_d^-| / (n_a^+ + n_d^+ + n_a^- + n_d^-)$ characterizes the asymmetry of the actin network. It has the value 0 when the network is completely symmetric and 1 when all filaments have only one orientation $+\theta_0$ or $-\theta_0$.

As shown in [3], the local dynamics (equations (2) with $y_x = 0$) gives rise to oscillations in the obstacle velocity for a large range of parameter values. The spatially extended model has a rich dynamics in this oscillatory regime. By varying v_p^{\max} , a and S , we found one regime where the membrane exhibits synchronous oscillations with periods between several seconds and 2 min (figure 4(A); see also supplementary material (available from stacks.iop.org/NJP/13/053040/mmedia) for movies of the corresponding membrane evolution.), and a second regime with a phase shift between different points of the oscillating membrane, resulting in laterally traveling waves (figures 4(B) and (C)), which are very similar to those measured by Döbereiner *et al* [1]. Both the experimental and the simulated waves show strong spatial and temporal modulation. The transitions between the three different protrusion regimes of the membrane—uniform protrusion, synchronous oscillations and traveling waves—are shown in figure 5. The solid lines mark a type I_0 linear instability [26]. Remarkably, traveling waves are found only for asymmetric networks, and the width of the parameter domain corresponding to traveling waves increases with increasing asymmetry and decreasing membrane tension. It can be shown that S and a scale the eigenspectrum of the linear problem like $\lambda(k; S, a) = \lambda\left(ak; \frac{S}{a^2}, 1\right)$, where $\lambda(k; S, a)$ is the complex eigenvalue corresponding to the wave number k . Hence, a parameter change along $a/\sqrt{S} = \text{const}$ cannot stabilize or destabilize the system, but influences only the spatial scale of the pattern.

The local dynamics exhibit regimes with an excitable steady state [27]. This gives rise to trigger waves (figures 4(C) and (D)) where a local protrusion of the flat, steadily moving membrane spreads to both sides along the membrane. We identify two cases: in figure 4(C), the protrusion splits into two waves traveling in opposite directions without changing shape; in figure 4(D) the perturbation remains localized around the initial site and increases in size, while small retractions arise periodically at its boundaries and travel to the center.

4. Conclusions

In summarize, we suggest that oscillations in bead and lamellipodium motion arise from the same mechanism, i.e. the interaction of forces, filament binding to the obstacle surface and free length dynamics in the polymer brush. The oscillation mechanism can be described as

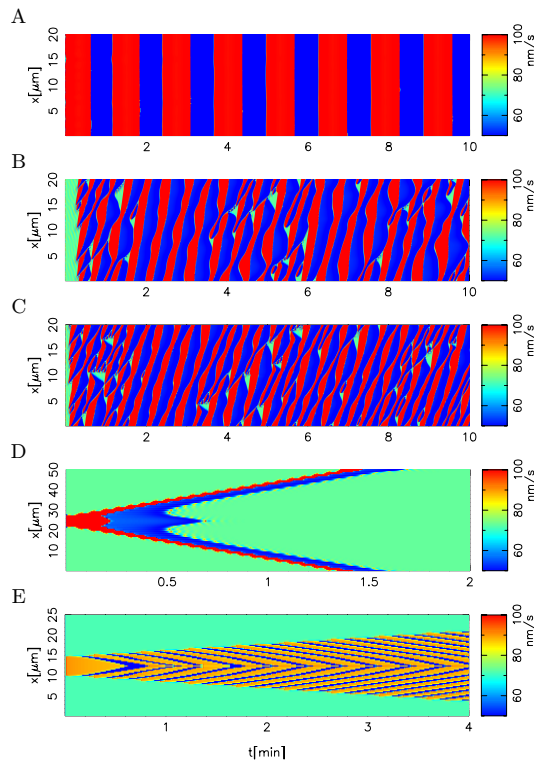


Figure 4. Normal velocity maps: (A) $v_p^{\max} = 7.5 \mu\text{m min}^{-1}$, $a = 0.5$, $S = 5 \text{ pN}$; (B) $v_p^{\max} = 8.4 \mu\text{m min}^{-1}$, $a = 0.5$, $S = 5 \text{ pN}$; (C) $v_p^{\max} = 8.4 \mu\text{m min}^{-1}$, $a = 0.8$, $S = 5 \text{ pN}$; (D) $v_p^{\max} = 9 \mu\text{m min}^{-1}$, $a = 0$, $S = 10 \text{ pN}$; (E) $v_p^{\max} = 6.6 \mu\text{m min}^{-1}$, $a = 0$, $S = 1 \text{ pN}$. Other parameters have the values given in table 1.

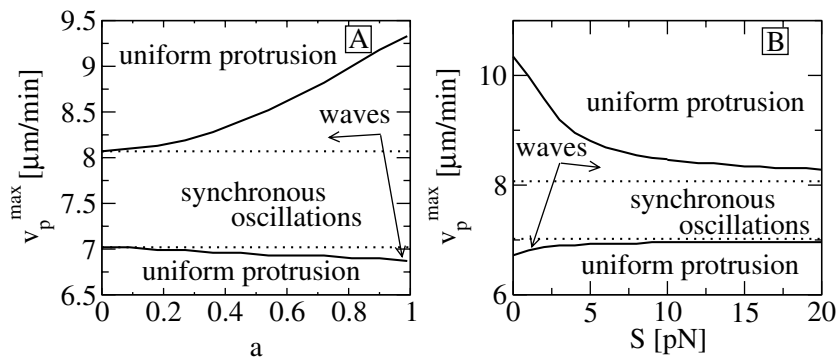


Figure 5. State diagrams of the motion of the membrane: (A) constant membrane tension $S = 10 \text{ pN}$; (B) constant asymmetry coefficient $a = 0.5$. Other parameters are the same as those in figure 4. Between dashed lines, synchronous oscillations like those in figure 4(A) are obtained. Between solid and dashed lines, traveling waves like those in figure 4(B) are obtained.

arising from instability against perturbations of the number of attached filaments. Decreasing the number of attached filaments increases the load on the remaining ones, accelerating their detachment. The pulling force $n_a F_a$ drops to very small values and the membrane or the bead

jerks forward. That relaxes all forces and re-attachment starts, thus closing the cycle (see [3, 27] for details). The essential difference between beads and lamellipodium is that beads experience much larger viscous forces due to actin gel almost enclosing them. We take this into account by a large effective drag coefficient η (see table 1).

Our mechanism for velocity oscillations of protein-coated beads shows very good agreement with experiments on oscillation periods and amplitudes, dependence of bifurcations on the protein surface density and bead diameter and the independence of bead velocity from diameter. An explanation of bead velocity oscillations based on an analysis of the elastic properties of the actin gel shows oscillations to arise from the escape of the bead from periodically formed stress on the bead surface [4]. Stress builds up because the gel is grown from a curved surface. The mechanism was compared to the escape of a piece of wet soap from a fist squeezing it [28]. The soap mechanism works for curved surfaces only. By contrast, our model predicts that oscillatory behavior is possible also in the case of flat obstacles [3, 27]. The oscillatory mechanism is therefore independent of the obstacle curvature. The particular geometry considered influences only the parameter values for the transition between steady and saltatory movements. We hope that our prediction will kindle future experiments for the study of the regime of motion for flat obstacles.

The soap mechanism relies on nonlinear friction for the generation of oscillations and predicts that the velocity in the steady regime decreases with increasing bead radius. Our mechanism, similarly to the soap mechanism, generates oscillations using linear friction, and predicts that the velocity does not depend on radius. The soap mechanism predicts that the maximum velocity of oscillations decreases in proportion to the diameter of beads. However, our mechanism predicts a decrease in amplitude with increasing diameter, reproducing the experimental data very well.

The ability of our mechanism to explain lamellipodial shape dynamics and its bifurcations beyond the examples given here has been shown recently [25] in a publication focusing on a comparison to the experiments reported in [2]. That includes also the waves corresponding to an excitable regime of the brush dynamics [27]. Simulations reproducing velocity oscillations observed with *Listeria* bacteria and oil droplets (including the onset of oscillations due to changes in the VASP concentration) have been presented in [3, 27]. The basic oscillation mechanism suggested by our model is the same for all these systems, but the parameter values are of course system specific. Coupling the model with the actomyosin gel in the bulk allows us to calculate the force velocity relation and stall forces, which are also in good agreement with experiments [17]. Hence, our model offers a unifying theory across several systems and experimental observations.

References

- [1] Döbereiner H-G, Dubin-Thaler B, Hofman J, Xenias H, Sims T, Giannone G, Dustin M, Wiggins C and Sheetz M 2006 Lateral membrane waves constitute a universal dynamic pattern of motile cells *Phys. Rev. Lett.* **97** 038102
- [2] Machacek M and Danuser G 2006 Morphodynamic profiling of protrusion phenotypes *Biophys. J.* **90** 1439–42
- [3] Gholami A, Falcke M and Frey E 2008 Velocity oscillations in actin-based motility *New J. Phys.* **10** 033022
- [4] Bernheim-Groswasser A, Prost J and Sykes C 2005 Mechanism of actin-based motility: a dynamic state diagram *Biophys. J.* **89** 1411–9

- [5] Michelot A, Berro J, Guerin C, Boujemaa-Paterski C, Staiger C J, Martiel J L and Blanchoin L 2009 Actin-filament stochastic dynamics mediated by ADF/cofilin *Curr. Biol.* **17** 825–33
- [6] Dayel M J, Akin O, Landeryou M, Risca V, Mogilner A and Mullins R D 2009 *In silico* reconstitution of actin-based symmetry breaking and motility *PLoS Biol.* **7** e1000201
- [7] John K, Peyla P, Kassner K, Prost J and Misbah C 2008 Nonlinear study of symmetry breaking in actin gels: implications for cellular motility *Phys. Rev. Lett.* **100** 068101
- [8] Cameron L A, Svitkina T M, Vignjevic D, Theriot J A and Borisy G G 2001 Dendritic organization of actin comet tails *Curr. Biol.* **11** 130–5
- [9] Bernheim-Groswasser A, Wiesner S, Golsteyn R M, Carlier M-F and Sykes C 2002 The dynamics of actin-based motility depend on surface parameters *Nature* **417** 308–11
- [10] Loisel T P, Boujemaa R, Pantaloni D and Carlier M-F 1999 Reconstitution of actin-based motility of *Listeria* and *Shigella* using pure proteins *Nature* **401** 613–6
- [11] Briehner W M, Coughlin M and Mitchison T J 2004 Fascin-mediated propulsion of *Listeria monocytogenes* independent of frequent nucleation by the Arp2/3 complex *J. Cell Biol.* **165** 233–42
- [12] Gholami A, Wilhelm J and Frey E 2006 Entropic forces generated by grafted semiflexible polymers *Phys. Rev. E* **74** 041803
- [13] Sechi A S, Wehland J and Victor Small J 1997 The isolated comet tail pseudopodium of *Listeria monocytogenes*: a tail of two actin filament populations, long and axial and short and random *J. Cell Biol.* **137** 155–67
- [14] Marcy Y, Prost J, Carlier M-F and Sykes C 2004 Forces generated during actin-based propulsion: a direct measurement by micromanipulation *Proc. Natl Acad. Sci. USA* **101** 5992–7
- [15] Mogilner A and Oster G 2003 Force generation by actin polymerization. II. The elastic ratchet and tethered filaments *Biophys. J.* **84** 1591–605
- [16] Evans E 2001 Probing the relation between force and chemistry in single molecular bonds *Ann. Rev. Biophys. Biomol. Struct.* **30** 105–28
- [17] Zimmermann J, Enculescu M and Falcke M 2010 Leading edge–gel coupling in lamellipodium motion *Phys. Rev. E* **82** 051925
- [18] Kroy K and Frey E 1996 Force–extension relation and plateau modulus for wormlike chains *Phys. Rev. Lett.* **77** 306–9
- [19] Kruse K, Joanny J F, Jülicher F, Prost J and Sekimoto K 2005 Active polar gels: a paradigm for cytoskeletal dynamics *Eur. Phys. J. E* **16** 5–16
- [20] Kruse K, Joanny J F, Jülicher F and Prost J 2006 Contractility and retrograde flow in lamellipodium motion *Phys. Biol.* **3** 130–7
- [21] Ebeling W and Feistel R 1986 *Physik der Selbstorganisation und Evolution* (Berlin: Akademie-Verlag)
- [22] Wiesner S, Helfer E, Didry D, Ducouret G, Lafuma F, Carlier M F and Pantaloni D 2003 A biomimetic motility assay provides insight into the mechanism of actin-based motility *J. Cell Biol.* **160** 387–98
- [23] Svitkina T, Verkhovskiy A, McQuade K and Borisy G 1997 Mechanism of cell body translocation *J. Cell Biol.* **139** 397–415
- [24] Verkhovskiy A B, Chaga O Y, Schaub S, Svitkina T M, Meister J-J and Borisy G 2003 Orientational order of the lamellipodial actin network as demonstrated in living motile cells *Mol. Biol. Cell* **14** 4667–75
- [25] Enculescu M, Sabouri-Ghomi M, Danuser G and Falcke M 2010 Modeling of protrusion phenotypes driven by the actin–membrane interaction *Biophys. J.* **98** 1–11
- [26] Cross M C and Hohenberg P C 1993 Pattern formation outside of equilibrium *Rev. Mod. Phys.* **65** 851–1123
- [27] Enculescu M, Gholami A and Falcke M 2008 Dynamic regimes and bifurcation in a model of actin-based motility *Phys. Rev. E* **78** 031915
- [28] Gerbal F, Chaikin P, Rabin Y and Prost J 2000 An elastic analysis of *Listeria monocytogenes* propulsion *Biophys. J.* **79** 2259–75
- [29] Mogilner A 2009 Mathematics of cell motility: have we got its number? *J. Math. Biol.* **58** 105–34
- [30] Le Goff L, Hallatschek O, Frey E and Amblard F 2002 Traces studies on f-actin fluctuations *Phys. Rev. Lett.* **89** 258101

- [31] Mogilner A and Oster G 1996 Cell motility driven by actin polymerization *Biophys. J.* **71** 3030–45
- [32] Abraham V C, Krishnamurthi D, Taylor D L and Lanni F 1999 The actin-based nanomachine at the leading edge of migrating cells *Biophys. J.* **77** 1721–32
- [33] Novak I L, Slepchenko B M and Mogilner A 2008 Quantitative analysis of g-actin transport in motile cells *Biophys. J.* **95** 1627–38
- [34] Koester S A, Auinger S, Vinzenz M, Rottner K and Small J V 2008 Differentially oriented populations of actin filaments generated in lamellipodia collaborate in pushing and pausing at the cell front *Nat. Cell Biol.* **10** 306–13